Ilioudis, Christos and Cao, Jianlin and Theodorou, Ilias and Striano, Pasquale and Coventry, William and Clemente, Carmine and Soraghan, John (2019) GNSS based passive radar for UAV monitoring. In: IEEE Radar Conference 2019, 2019-01-22 - 2019-01-26, Westin Waterfront Hotel. ,

This version is available at https://strathprints.strath.ac.uk/67270/

GNSS Based Passive Radar for UAV Monitoring

Christos V. Ilioudis, Jianlin Cao, Ilias Theodorou, Pasquale Striano
William Coventry, Carmine Clemente and John Soraghan
Department of Electronic and Electrical Engineering
University of Strathclyde Glasgow, UK
Email: {c.ilioudis, jianlin.cao, ilias.theodorou, pasquale.striano, william.coventry, carmine.clemente, j.soraghan}@strath.ac.uk

Abstract—**Monitoring of unmanned aerial vehicle (UAV) targets has been a subject of great importance in both defence and security sectors. In this paper a novel system is introduced based on a passive bistatic radar using Global Navigation Satellite Systems (GNSS) as illuminators of opportunity. Particularly, a link budget analysis is held to determine the capabilities and limitations of such a system. Additionally, a signal reconstruction algorithm is provided allowing estimation of the transmitted signal from each satellite. Finally, the proposed system is tested in outdoor acquisitions of small UAV targets where the Fractional Fourier Transform (FrFT) is used as tool to enhance target detectability.**

Index Terms—**GNSS, Passive Radar, UAV, Forward Scattering**

I. INTRODUCTION

In the literature, passive bistatic radar (PBR) systems have been widely suggested for a variety of applications [1]–[10]. While generally having more limitations compared to active radars, PBR systems offer an attractive monitoring solution due to their lower operational cost and no need of frequency allocation. Additionally, since PBR have no emissions, they are hard to be detected and therefore avoided by the target. Recently, due to vast rising number of civilian and commercial unmanned aerial vehicles (UAV), a significant interest of the radar engineering community has been focused on PBR architectures for UAV monitoring. Particularly, systems exploiting digital television [1], digital audio broadcasting [2] and mobile communication [3] illuminators of opportunity (IO) have been previously suggested.

Traditionally, PBR systems comprise a reference channel, used to acquire the direct IO signal, and a surveillance channel that captures the electromagnetic (EM) returns from potential targets. As a special case of PBR, the forward scattering radar (FSR) configuration occurs when the target crosses (or is very close to) the line of sight between the IO and the passive receiver. In this special case, the detection of a target is done by the EM "shadow" that the target casts on the receiver rather than its reflection. This make FSR particularly attractive for targets with low reflectivity, as their "shadow" is mainly dependent on the silhouette of the target and not by its material.

Recent developments show that FSR systems have gained traction in the research community. Namely, in [4] and [5] the authors investigated and later validated in [6] the capability of a GNSS PBR system to extract micro-Doppler signatures of helicopter targets when operating in near FSR configuration. Moreover, in [7] the Doppler information extraction in a GNSS based FSR was validated, while the authors in [8] suggested a filter bank based algorithm that is able to estimate range and velocity parameters of the moving target.

In [9] a GNSS based PBR was proposed for synthetic aperture radar (SAR) applications using a synchronization algorithm to generate the reference, satellite, signal at the receiver. Based on the same principles, the authors in [10] proposed and experimentally validated a GNSS PBR system design for maritime target detection. Furthermore, link budget studies for airborne targets detection using GPS PBR was held in [11] referring to the shortcomings of such systems due to the high direct signal and clutter returns.

In this work a PBR exploiting GNSS IOs is proposed for monitoring of UAV targets. More specifically, the system aims to capture returns from small airborne targets and if available exploit the FSR configuration in order to enhance its detection capabilities. Additionally, a signal reconstruction algorithm is presented in order to estimate and generate the appropriate receiver filters based on the direct GNSS signal. The detection performance of the system is examined through link budget analysis and experimental acquisitions. Additionally, a time-frequency analysis based on the fractional Fourier transform (FrFT) is also employed in order to improve the target detection performance of the proposed system.

The remainder of the paper is organised as follows. Section II describes the proposed system configuration with focus on the forward scattering phenomenology and provides a link budget analysis. Section III discusses the examined signal model while Section IV presents the proposed signal reconstruction algorithm. In Section V experimental results validating the system are discussed. Finally, Section VI concludes the paper.

II. FORWARD SCATTERING

The examined system topology is illustrated in Fig. 1. As it can be seen, the configuration comprises a satellite IO Tx, a ground passive receiver with two channels Hx and Rx, and an airborne target Tg, with their distances being denoted as: D_S satellite to receiver, D_T satellite to target, and D_R target to receiver. As the signal is transmitted from the satellite to earth, portion of it is directly received by Hx while another part first reaches Tg and is then scattered at different directions.
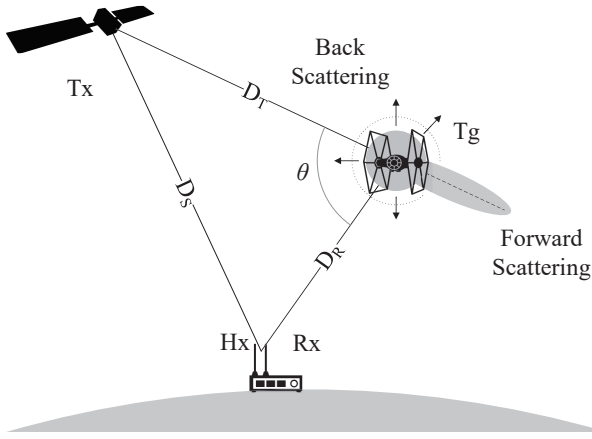
Fig. 1. Examined passive GNSS radar topology comprising a satellite IO Tx, a UAV target Tg, and a two channel receiver Hx and Rx.

	Description		GPS	Galileo
λ	Wavelength	[cm]	19.03	19.03
$D_\mathcal{T}$	Satellite to target distance	[km]	20200	33000
$P_\mathcal{T}$	Transmitted power (mean)	[dBW]	20.5	23.5
$\hat{P}_\mathcal{T}$	Transmitted power (max)	[dBW]	23.8	24.2
$\check{P}_\mathcal{T}$	Transmitted power (min)	[dBW]	17	22
$G_\mathcal{T}$	Transmitter gain	[dBi]	15	16.5
T	Code duration	[ms]	1	4
B_s	Code bandwidth	[MHz]	1.023	1.023
$G_\mathcal{P}$	Signal processing gain	[dB]	30.1	36.1
$G_\mathcal{R}$	Receiver gain	[dBi]	36	36
L_s	Losses	[dB]	-3	-3
$\hat{\rho}$	Minimum SNR for detection	[dB]	10	10
T_0	Noise reference temperature	[K]	290	290
B_r	Receiver bandwidth	[MHz]	4	4
F	Receiver noise figure	[dB]	10	10

Depending on the configuration, Rx will capture the reflections from the target in different scattering directions. Particularly, depending on the bistatic angle θ three distinct radar cross section (RCS) regions are distinguished: pseudo-monostatic at $\theta < 20°$, back scattering (BS) at $20° < \theta < 140°$, and forward scattering (FS) at $\theta > 140°$. As described in [12], the FS effect can significantly increase the target's RCS in the forward direction. Since higher RCS leads to better detection, here the forward scattering cross section (FSCS) will be considered as optimum case for the examined scenario.

An overview on the phenomenology of FSCS is provided in [13]. In the present analysis, small UAV targets are considered with typical dimension d varying between 0.25 and 0.5m. This dimension was chosen based on the maximum span of the targets main body. For the IO, the L1 frequency (1575.42 MHz) of the GPS signal is of focus, corresponding to a wavelength $\lambda = 0.19$m. Using these values, it can be calculated that the ratio d/λ takes values between 1.3 and 2.6, meaning that the targets will fall into the late Mie and early optical scattering region where enhancement of the RCS in the FS direction becomes more significant [13]. The maximum FSCS in the optical region can be calculated from [14]:

$$\sigma_{\max} = 4\pi A^2/\lambda^2 \tag{1}$$

where A is the physical area of the target. In practice, this maximum value can only be achieved if the receiver antenna falls into the forward scattering main lobe. This lobe is centered across the line of site between the transmitter and target facing the opposite direction from the transmitter, see Fig. 1, while its width is proportional to λ and inversely proportional to d [13].

A. Link Budget

One of the main objectives of this work is to investigate the performance capabilities and limitations of a GNSS based FS radar. For this reason, a preliminary estimation of the required link budget is performed. The figure of merit for this analysis

is the signal to noise ratio (SNR), which for a single pulse in the surveillance channel is [11], [15]:

$$\rho = \left(\frac{P_\mathcal{T} G_\mathcal{T}}{4\pi D_\mathcal{T}^2}\right)\left(\frac{\sigma}{4\pi D_\mathcal{R}^2}\right)\left(\frac{\lambda^2 G_\mathcal{R} L_s}{4\pi}\right)\frac{G_\mathcal{P}}{P_n} \tag{2}$$

where $P_\mathcal{T}$ is the transmitted power of the IO, $G_\mathcal{T}$ and $G_\mathcal{R}$ are the total gains, antenna plus amplifier, in the transmission and reception respectively, σ is the RCS of the target, L_s denotes any no free-space propagation losses, $G_\mathcal{P}$ is the signal processing gain given by the time bandwidth product of the signal [16], and P_n is the power of the noise; calculated as:

$$P_n = kT_0 B_r F \tag{3}$$

with k being the Boltzmann's constant, T_0 is the noise reference temperature, B_r is the receiver bandwidth and F is the receiver noise figure. To enhance the performance, incoherent integration of duration T_I is also considered, where the improved SNR is given as:

$$\hat{\rho} = \sqrt{\frac{T_I}{T}}\rho \tag{4}$$

with T being the duration of the code used by the satellite.

Rearranging (2) it is possible to express the maximum detectable range for a certain set of configurations. The values for each parameter where selected according to [17] and are summarised in Table I. Particularly, two satellite constellations are considered; GPS and Galileo. For each constellation the mean power is calculated as the total transmitted power divided by the number of satellites, and the maximum and minimum as the highest and lowest power transmitted from an individual satellite out of the constellation. Moreover, $\hat{\rho}$ is set to the minimum SNR for the system to be able to perform detection while the RCS of the target is calculated using (1) where the area is approximated by a disk, i.e. $A = \pi(d/2)^2$.

The minimum detectable range versus the characteristic dimension of the target for both constellations is illustrated in Fig. 2. Additionally error bars have been included to account
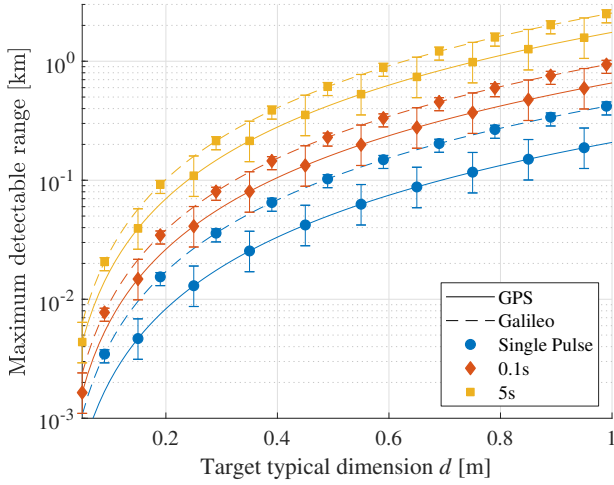
Fig. 2. Maximum detectable range versus d for two satellite constellations and different incoherent integration time intervals.

for the higher and lower achievable ranges when the maximum and minimum transmitted powers are considered respectively. Examining the result, it can be seen the Galileo constellation allows detection in higher ranges than the GPS. Particularly, for Galileo a target with typical dimension $d = 0.5$ m is possible to be detected at 240 m for 0.1 s of integration and 630 m for 5 s, while for GPS the respective values are 160 and 440 m. It is worth noting that for the Galileo constellation the higher and lower ranges are much closer to the mean values compared to the GPS. This is expected as the maximum and minimum transmitted powers are much closer to the mean for Galileo.

III. SIGNAL MODEL

Considering a constant transmitter-receiver channel and not accounting for propagation losses, the direct path signal from the i-th GNSS satellite at the passive receiver can be expressed in intermediate frequency as:

$$r_i(t) = m_i(t - \tau_i)g_i(t - \tau_i)e^{j[2\pi f_i t + \phi_i + \psi_i]} \quad (5)$$

where $m_i(t)$ denotes the navigation message and $g_i(t)$ is a Pseudorandom Noise (PRN) code sequence. Additionally τ_i, f_i and ϕ_i are the signal's time, frequency and phase shifts respectively caused due to the distance and relative velocity between the satellite and the receiver, and ψ_i is a phase error caused by non- free-space propagation phenomena such as hardware imperfections.

As the PRN code is known by the receiver and is hence used for the detection of the signal, it is useful to define its duration as the Pulse Repetition Interval (PRI) of the transmitter which equals to $\text{PRI} = N_c T_c$, where N_c and T_c are the number and duration of each code chip. The time between the beginning and the end of each PRI, i.e. $t \in [0, \text{PRI}]$ is also commonly referred to as *fast-time*, while the time intervals with duration of a PRI, i.e. $u = 0, \text{PRI}, 2\text{PRI}, ...$ are referred to as *slow-time*. Furthermore, while (5) provides a useful description of the received signal, in reality the channel cannot be considered constant throughout long periods of time. A reasonable assumption however would be to model the delay, frequency shift and phase error to vary in slow-time, i.e. $\tau_i(u)$, $f_i(u)$ and $\psi_i(u)$. The received signal in (5) can therefore be remodeled as:

$$r_i(t, u) = m_i(u)g_i(t, u)e^{j[2\pi f_i(u)(t+u)+\phi_i(u)+\psi_i(u)]} \quad (6)$$

where the different components are given as:

$$m_i(u) = m_i\big(\tau_i(u)\big) \quad (7)$$
$$g_i(t, u) = g_i\big(t - \tau_i(u)\big) \quad (8)$$
$$\phi_i(u) = 2\pi\big(f_0 + f_i(u)\big)\tau_i(u) \quad (9)$$

where f_0 denotes the carrier frequency. It is worth noting that since $T_m \gg T_c$ where T_m is the duration of $m_i(t)$, the navigation message has also been modelled in slow time.

Following the model in (6), the return signal from a target can be expressed as:

$$\hat{r}_i(t, u) = \hat{m}_i(t, u)\hat{g}_i(t, u)e^{j[2\pi \hat{f}_i(u)(t+u)+\hat{\phi}_i(u)+\hat{\psi}_i(u)]} \quad (10)$$

where $\hat{\tau}_i(u)$, $\hat{f}_i(u)$ and $\hat{\psi}_i(u)$ are the delay, frequency shift and phase error that the signal experiences in the satellite-target-receiver path. The parameters $\hat{m}_i(t, u)$, $\hat{g}_i(t, u)$ and $\hat{\phi}_i(u)$ can be calculated similarly to their counterparts for the direct path propagation, see (7), (8) and (9) respectively, by substituting $\tau_i(u)$ with $\hat{\tau}_i(u)$ and $f_i(u)$ with $\hat{f}_i(u)$.

IV. SIGNAL RECONSTRUCTION ALGORITHM

In contrast to active radars, PBR commonly do not have a prior knowledge of the reference signal, making the need of a signal reconstruction process necessary. The adopted signal reconstruction algorithm is based on the synchronisation algorithm proposed in [9] with its basic operations being outlined in Fig. 3. For its input, the system utilises two channels: a reference channel, usually employing an omni-directional antenna and a surveillance channel using a more directional antenna. The input from the reference channel is used to estimate the transmitted signal from the considered
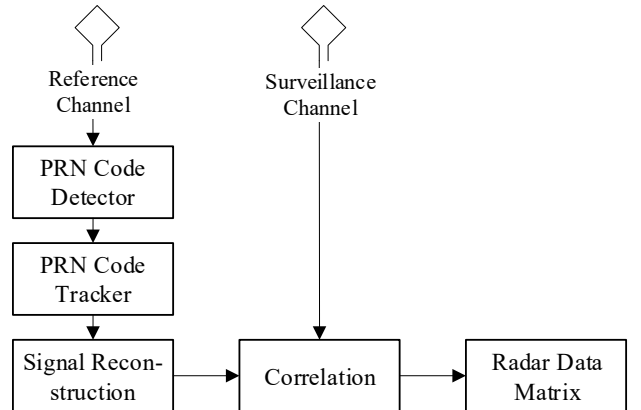

Fig. 3. Signal reconstruction algorithm.

IO, which in turn will be used to identify target scatterings in the surveillance channel through a correlation processes.

In the presented system, since GNSS IOs are exploited, multiple sources are expected to illuminate the surveillance area at the same time. As the IOs will have different positions and velocities it is important to separate their reference signals before correlating the two channels. For this reason a standard PRN code detector is used to identify the available satellites. During this process a segment of the reference channel's signal is correlated with different PRN sequences in order to approximate the delay and frequency shift of each satellite signal at the receiver. This information is then passed to a tracker which can provide a more accurate estimation of the delay and frequency shift while also filtering the signal with the PRN code. Using the outputs of the tracker, the signal from the satellite of interest can then be reconstructed and correlated with the signal from the surveillance channel in order to detect target scatterings.

Using the signal model derived in Section III, the signal at the reference and surveillance channels can be expressed as:

$$r_R(t, u) = \sum_{i=1}^{N_i} \sqrt{a_{i,R}(u)} r_i(t, u)$$
$$+ \sum_{i=1}^{N_i} \sqrt{\hat{a}_{i,R}(u)} \hat{r}_i(t, u) + n_R(t, u) \quad (11)$$

$$r_S(t, u) = \sum_{i=1}^{N_i} \sqrt{a_{i,S}(u)} r_i(t, u)$$
$$+ \sum_{i=1}^{N_i} \sqrt{\hat{a}_{i,S}(u)} \hat{r}_i(t, u) + n_S(t, u) \quad (12)$$

where $a_{i,R}(u)$, $\hat{a}_{i,R}(u)$ represent the power losses in the reference channel owing to the satellite-receiver and satellite-target-receiver paths, and $a_{i,S}(u)$ and $\hat{a}_{i,S}(u)$ are the respective losses in the surveillance channel. For the detector and tracker to work properly, the direct satellite signal must be dominant in the reference channel, i.e.:

$$a_{i,R}(u) \gg \hat{a}_{i,R}(u) \quad (13)$$

If (13) is satisfied, the tracker can provide an estimate of the delay $\tilde{\tau}_i(u) \approx \tau_i(u)$, frequency shift $\tilde{f}_i(u) \approx f_i(u)$ and phase shift $\tilde{\phi}_i(u) \approx \phi_i(u)$ that the signal experiences in the satellite-receiver path. Moreover the tracker outputs an estimate of the navigation signal:

$$\tilde{m}_i(u) = m_i(u - \tilde{\tau}_i(u)) e^{j2\pi\tilde{\psi}_i(u)} \quad (14)$$

where $\tilde{\psi}_i(u)$ is the phase error due to non-perfect code filtering and non- free-space propagation phenomena. Using this information, the signal from the i-th satellite can be reconstructed as:

$$\tilde{r}_{i,D}(t, u) = \tilde{m}_i(u)\tilde{g}_i(t, u) e^{j[2\pi\tilde{f}_i(u)(t+u) + \tilde{\phi}_i(u)]} \quad (15)$$

where $\tilde{g}_i(t, u) = g_i(t - \tilde{\tau}_i(u))$ is the time shifted PRN code.

After generating the reconstructed signal in (15) the system correlates it with the signal from the surveillance channel. By design, the signals transmitted from different satellites are orthogonal, thus the cross correlation between the reconstructed signal (15) and the surveillance channel (12) can be expressed as:

$$Y_i(k, u) = \int_0^{\text{PRI}} \tilde{r}_{i,D}^\dagger(t - k, u) r_S(t, u) \mathrm{d}t \quad (16)$$
$$= y_i(k, u) + \hat{y}_i(k, u) + n_i(k, u) \quad (17)$$

where $(\cdot)^\dagger$ denotes the complex conjugate operation, and $y_i(k, u)$, $\hat{y}_i(k, u)$, $n_i(k, u)$ are the correlation output components associated with the direct signal, target returns and noise respectively:

$$y_i(k, u) = \sqrt{a_{i,S}(u)} \int_0^{\text{PRI}} \tilde{r}_{i,D}^\dagger(t - k, u) r_i(t, u) \mathrm{d}t \quad (18)$$

$$\hat{y}_i(k, u) = \sqrt{\hat{a}_{i,S}(u)} \int_0^{\text{PRI}} \tilde{r}_{i,D}^\dagger(t - k, u) \hat{r}_i(t, u) \mathrm{d}t \quad (19)$$

$$n_i(k, u) = \int_0^{\text{PRI}} \tilde{r}_{i,D}^\dagger(t - k, u) n_S(t, u) \mathrm{d}t \quad (20)$$

Assuming an accurate reconstruction of the signal, and if $\tilde{\psi}_i(u) \approx \psi_i(u)$, (18) and (19) can be rewritten as:

$$y_i(k, u) = \sqrt{a_{i,S}(u)} \mathcal{A}(k, 0) \quad (21)$$

$$\hat{y}_i(k, u) = \sqrt{\hat{a}_{i,S}(u)} \mathcal{A}(\Delta\tau_i(u) + k, \Delta f_i(u)) \quad (22)$$

where $\mathcal{A}(\tau, f)$ is the *ambiguity function* of the PRN code at a delay τ and frequency shift f, and $\Delta\tau_i(u) = \tau_i(u) - \tilde{\tau}_i(u)$ and $\Delta f_i(u) = f_i(u) - \tilde{f}_i(u)$ represent the bi-static delay and Doppler shift respectively. Examining (21) and (22) it can be seen that the output from the filtered signal $Y_i(k, u)$ will have two main responses: one at zero delay and zero Doppler and one at $\Delta\tau_i(u)$ and $\Delta f_i(u)$. If $\Delta\tau_i(u) \neq 0$ or $\Delta f_i(u) \neq 0$ it is therefore possible to estimate the target's range and velocity after de-cluttering the signal.

V. EXPERIMENTAL VALIDATION

To validate the proposed system, outdoor experiments were performed to acquire real GNSS data in presence of UAV targets. The passive receiver was implemented using a Software Defined Radio (SDR) device [18]. For the reference channel, a conical shaped GPS L1 antenna was employed, while a flat panel antenna was used for the surveillance channel. The processing of the signal was done offline using a MATLAB implementation of the algorithm described in Section IV. Particularly for the detection of the code an implementation of the FFT search was used, while the tracking was performed via a coupled code and carrier tracking loop [19].

The acquisitions were held at the Caplaw Model Flying Group premises at Glasgow, UK while the target was a DJI Phantom 4 which has an approximate maximum span of 409.4 mm [20]. The location of the satellites during the acquisition is provided in Fig. 4a Additionally, in Fig. 4b the peak to average ratio (PAR) of the maximum PRN code correlation response in different frequency shifts is provided for each satellite. High PAR generally yields correct detection of the satellite signal and therefore is used as a criterion the presented system.

(a) Satellite Position
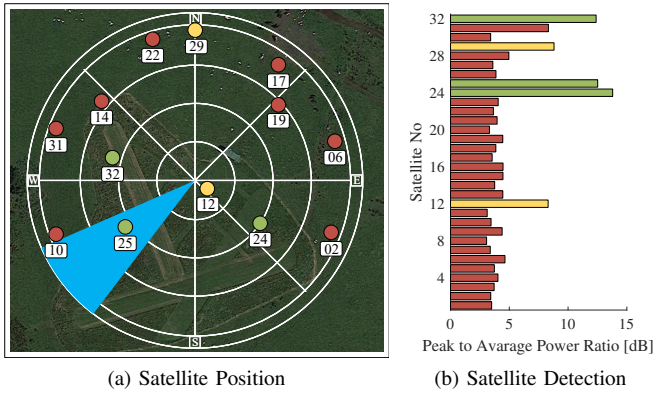
(b) Satellite Detection

Fig. 4. Field map overlaid with the satellites' position above the horizon and surveillance antenna's main beam (a) and peak to average power ratio of each satellite in the reference channel (b).
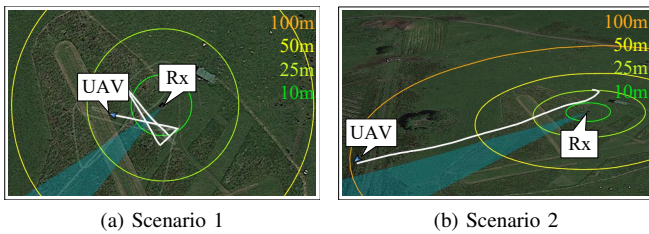

(a) Scenario 1

(b) Scenario 2

Fig. 5. UAV fight path and different range indicators from the radar position.

A. Scenario 1: Close crossing

In the first examined scenario the radar returns will be evaluated for the UAV target doing several crossings in front of the surveillance antenna. The target flight path is shown in Fig. 5a. To examine the system in a FS configuration the satellite No.25 was chosen as it provides the highest PAR in the desired direction. The spectrogram of the received signal calculated using the short-time Fourier transform (STFT) and normalising by the maximum value is illustrated in Fig. 6a. As it can be seen when the target is present in the surveillance channel, returns in non-zero Doppler arise. It should be noted that the signal is passed through a high pass filter to mitigate the direct signal and clutter components. For comparison the spectrogram when the satellite No.24 is provided in Fig. 6b. As it can be seen, when a different satellite is used, the target appears in different frequency shifts. This is expected as the bistatic Doppler is highly dependent in the geometry of the system. Additionally, comparing Fig. 6a and Fig. 6b it can be seen that the FS case provides lower noise floor.

B. Scenario 2: Departing

In the second examined scenario, the target is moving away from the radar while remaining inside the surveillance antenna beam. The target flight path is shown in Fig. 5b. Particularly, the acquisition starts with the target behind the surveillance antenna, it then moves in-front of it and flies away in a straight line. In Fig. 7a the spectrogram generated with a 5s window is illustrated. As it can be seen the at 8s a positive
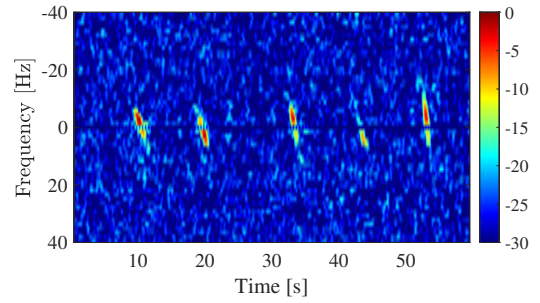
(a) Satellite No.25
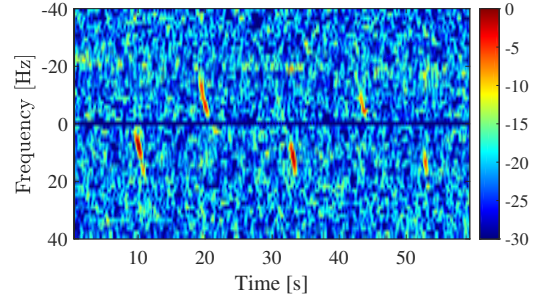
(b) Satellite No.24

Fig. 6. Spectrogram of captured signal at 0 range bin for 1s window duration using satellite (a) No.25 and (b) No.24.

Doppler component is present, with the frequency increasing until 12.5s and then disappearing. Associating the results with the examined scenario, the UAV can be detected approximately up to 100m away from the radar.

Comparing the results with those of a smaller time window, see Fig. 6, it can be seen that increasing the window size has improved the frequency resolution, trading however with higher noise floor level. As it can be seen in Fig. 7a, the target's returns exhibit a near linear frequency modulation. This is caused due to change of the relative velocity between the receiver and the target as the target moves away from the receiver. This frequency modulation causes the signal to spread in multiple frequency bins. This "defocussing" becomes more apparent as the time window increases. In order to cope with this phenomenon, an analysis based on the fractional Fourier transform (FrFT) is also employed. The FrFT is a generalisation of the traditional Fourier transform (FT) finding many applications in signal processing [21]. While the FT is considered as a translation of a signal from the time to frequency axes, when those axes are placed perpendicular the FrFT can be interpreted as a rotation of a signal in the time-frequency plane. Consequently, when this rotation is equal to π the FrFT results to the conventional FT.

A spectrogram-like illustration based on the short-time FrFT (STFrFT) is referred to as *slanted spectrogram* and is calculated by replacing the FT with the FrFT in the STFT and picking the rotation angle with the maximum response [22]. The slanted spectrograms of the received signal us illustrated in Fig. 7b. Comparing Fig. 7a and Fig. 7b it can be seen that the noise level has been reduced and the signal is localised

(a) 1s Window Duration
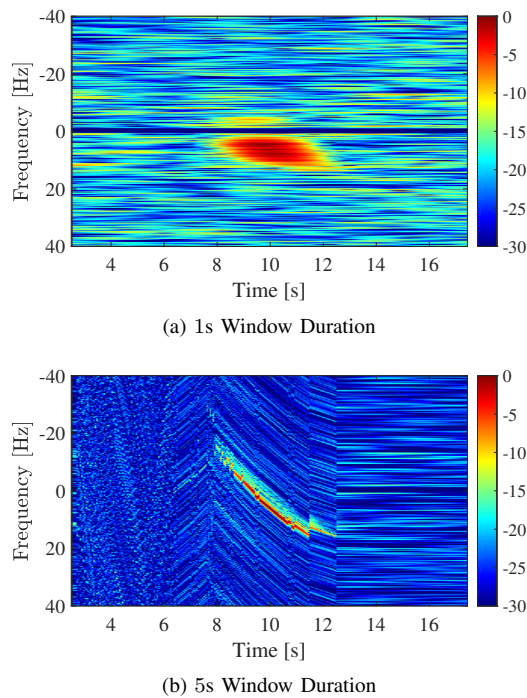

(b) 5s Window Duration

Fig. 7. Spectrogram (a) and slanted spectrogram (b) of captured signal at 0 range bin calculated using 5s window duration.

better. To quantify the localisation improvement, the peak to average ratio (PAR) of different frequency bins in the same time window was used as a figure of merit. Particularly, for the time span that the target is present, i.e. 8s to 12.5s, the mean PAR for the conventional and slanted spectrograms are 24.1 and 46.5 respectively. As higher PAR generally indicate lower noise floor levers, it is show that the FrFT method offers better localisation performance.

VI. Conclusion

The presented work investigated the monitoring capabilities of a GNSS based PBR system in small UAV targets scenarios. Particularly a link budget analysis was held for two GNSS constellations indicating the ability to significantly improve the detectable ranges when high power satellites and linger integration times are considered. The proposed system was evaluated though experimental acquisitions in different flight path scenarios. The results demonstrated the ability of the system to detect a small UAV target up to 100m away from the receiver. Lastly the STFrFT was used in order to improve the target parameter estimation capabilities of the systems. In future analysis, captures from different satellite constellations, such as Galileo, will be examined while utilisation of combined satellite returns will also be investigated in order to improve the detection and localisation performance.

Acknowledgment

References

[1] Y. Liu, X. Wan, H. Tang, J. Yi, Y. Cheng, and X. Zhang, "Digital television based passive bistatic radar system for drone detection," in *2017 IEEE Radar Conference (RadarConf)*, May 2017, pp. 1493–1497.

[2] C. Schpbach, C. Patry, F. Maasdorp, U. Bniger, and P. Wellig, "Micro-uav detection using dab-based passive radar," in *2017 IEEE Radar Conference (RadarConf)*, May 2017, pp. 1037–1040.

[3] B. Knoedler, R. Zemmari, and W. Koch, "On the detection of small uav using a gsm passive coherent location system," in *2016 17th International Radar Symposium (IRS)*, May 2016, pp. 1–4.

[4] C. Clemente and J. J. Soraghan, "Passive bistatic radar for helicopters classification: A feasibility study," in *2012 IEEE Radar Conference*, May 2012, pp. 0946–0949.

[5] C. Clemente and J. J. Soraghan, "Gnss-based passive bistatic radar for micro-doppler analysis of helicopter rotor blades," *IEEE Transactions on Aerospace and Electronic Systems*, vol. 50, no. 1, pp. 491–500, January 2014.

[6] C. Clemente, T. Parry, G. Galston, P. Hammond, C. Berry, C. Ilioudis, D. Gaglione, and J. J. Soraghan, "Gnss based passive bistatic radar for micro-doppler based classification of helicopters: Experimental validation," in *2015 IEEE Radar Conference (RadarCon)*, May 2015, pp. 1104–1108.

[7] C. Liu, C. Hu, R. Wang, X. Nie, and F. Liu, "Gnss forward scatter radar detection: Signal processing and experiment," in *2017 18th International Radar Symposium (IRS)*, June 2017, pp. 1–9.

[8] A. D. Luca, L. Daniel, M. Gashinova, and M. Cherniakov, "Target parameter estimation in moving transmitter moving receiver forward scatter radar," in *2017 18th International Radar Symposium (IRS)*, June 2017, pp. 1–7.

[9] M. Antoniou and M. Cherniakov, "Gnss-based bistatic sar: a signal processing view," *EURASIP Journal on Advances in Signal Processing*, vol. 2013, no. 1, p. 98, May 2013. [Online]. Available: https://doi.org/10.1186/1687-6180-2013-98

[10] H. Ma, M. Antoniou, M. Cherniakov, D. Pastina, F. Santi, F. Pieralice, and M. Bucciarelli, "Maritime target detection using gnss-based radar: Experimental proof of concept," in *2017 IEEE Radar Conference (RadarConf)*, May 2017, pp. 0464–0469.

[11] Y. Wu, W. Qu, H. Wang, X. Jia, and S. Ji-liang, "Study on bistatic (multi) radar system using navigation satellites," in *2008 8th International Symposium on Antennas, Propagation and EM Theory*, Nov 2008, pp. 1286–1289.

[12] N. J. Willis, *Bistatic radar*. SciTech Publishing, 2005, vol. 2.

[13] M. Gashinova, L. Daniel, E. Hoare, V. Sizov, K. Kabakchiev, and M. Cherniakov, "Signal characterisation and processing in the forward scatter mode of bistatic passive coherent location systems," *EURASIP Journal on Advances in Signal Processing*, vol. 2013, no. 1, p. 36, 2013.

[14] M. Skolnik, *Radar Handbook, Third Edition*, ser. Electronics electrical engineering. McGraw-Hill Education, 2008.

[15] A. R. Persico, P. Kirkland, C. Clemente, M. Vasile, and J. J. Soraghan, "Cubesat-based passive bistatic radar for space situational awareness: A feasibility study," *IEEE Transactions on Aerospace and Electronic Systems*, pp. 1–1, 2018.

[16] M. A. Richards, J. A. Scheer, W. A. Holm, B. Beckley, P. Mark, A. Richards *et al.*, "Principles of modern radar volume i-basic principles," 2010.

[17] P. Steigenberger, S. Thoelert, and O. Montenbruck, "Gnss satellite transmit power and its impact on orbit determination," *Journal of Geodesy*, vol. 92, no. 6, pp. 609–624, Jun 2018. [Online]. Available: https://doi.org/10.1007/s00190-017-1082-2

[18] National Instruments, "Usrp-2943 software defined radio reconfigurable device," ni.com/pdf/manuals/374193d.pdf, Accessed: 2018-08-06.

[19] J. B.-Y. Tsui, *Fundamentals of global positioning system receivers: a software approach*. John Wiley & Sons, 2005, vol. 173.

[20] DJI, "Dji phantom 4 specifications," geodirect.nl/assets/productsheets/DJI-Phantom-4-Datasheet.pdf, Accessed: 2018-08-06.

[21] H. M. Ozaktas and M. A. Kutay, "The fractional fourier transform," in *Control Conference (ECC), 2001 European*. IEEE, 2001, pp. 1477–1483.

[22] O. Agcaoglu, B. Santhanam, and M. Hayat, "Improved spectrograms using the discrete fractional fourier transform," in *2013 IEEE Digital Signal Processing and Signal Processing Education Meeting (DSP/SPE)*, Aug 2013, pp. 80–85.